Full-Range Soft-Switching Pulse Frequency Modulated Wireless Power Transfer

Wei Liu, *Student Member, IEEE*, K. T. Chau, *Fellow, IEEE*, Christopher H. T. Lee, *Senior Member, IEEE*,
Wei Han, *Student Member, IEEE*, Xiaoyang Tian, *Student Member, IEEE*,
and W. H. Lam, *Senior Member, IEEE*

***Abstract*—This article proposes and implements a full-range soft-switching pulse frequency modulated (PFM) wireless power transfer (WPT) system, which not only offers high efficiency but also high controllability, selectivity, and security. Although the phase-shift control (PSC) has been widely used in various WPT applications, the high-frequency hard-switching operation will inevitably degrade the system performances in terms of power losses, and hence, efficiency during power regulation. Thus, a soft-switching PFM is newly conceived to suppress the switching frequency and power losses while maintaining full-range soft switching for effective power control, hence improving the system efficiency. In addition to realizing the controllability, the full-range soft-switching PFM can be further derived to implement the selectivity and security. The system efficiency of a multiobjective PFM-WPT system prototype can reach 86.27% at 220-W output power and 135-mm transfer distance. During wireless power control, it can effectively be improved by up to 5.68% as compared to its counterpart using the PSC. Theoretical analysis, computer simulation, and hardware experimentation are given to verify the feasibility of proposed full-range soft-switching PFM-WPT system.**

***Index Terms*—Controllability, pulse frequency modulation (PFM), security, selectivity, soft-switching, wireless power transfer (WPT).**

I. INTRODUCTION

NIKOLA Tesla has pioneered the concept of wireless power transfer (WPT) more than one century ago. In various industrial applications and interdisciplinary areas, the WPT using magnetic resonant coupling (MRC) has got extensively investigated and gradually applied in the last decade [1]. As one of the most epoch-making technologies, the WPT technology has fully exhibited its key advantages of better safety and convenience, stronger reliability and electrical isolation, and less maintenance [2]. As a result, it has been attracting a growing number of academic researchers and industries to get involved in the great explorations and attempts, such as the static and dynamic wireless charging flexibility [3], [4], wireless energy selectivity [5], [6], and emerging wireless energy security [7], [8].

The practical requirement on wireless power controllability may be raised in diverse WPT applications, such as wireless battery charging management [9], wireless motor speed regulation [10], and wireless dimming control. Taking into account wireless power adjustment in the areas of the WPT-based power electronics, the control strategies can generally fall into three mainstream techniques, which are pulsewidth modulation (PWM), pulse density modulation (PDM), and pulse frequency modulation (PFM). First, the phase-shift control (PSC) [9], [11] is widely used to offer the desired gate signals for full-bridge inverters or active rectifiers in various WPT systems. It can be theoretically classified as a kind of PWM with a controllable duty ratio on the inverter output. The PSC takes the key merit of simplicity. However, when varying the duty ratio for power adjustment, the initial soft-switching operation will be deteriorated unless using a complicated zero-voltage-switching (ZVS) angle control [9]. Hence, the constant high-frequency hard switching may degrade the system performance in terms of power and efficiency losses during power regulation. Second, three alternative methods of the burst firing control [12], ON–OFF keying modulation [13], and three-level relay control incorporating with high-frequency modulation [14] can be essentially regarded as the PDM [15]. They can competently output a controllable wireless power with low but nonnegligible subharmonics. Third, the MRC-based WPT system usually requires an involved inverter to operate at high-frequency switching for maintaining high-efficiency transmission. The reported WPT scheme using energy injection [16] or harmonic currents [17], [18] operates at a fixed low-frequency switching to transfer the high-frequency resonant wireless energy. However, it may suffer from significant output fluctuations or relatively high voltage stress with the same power level. In this article, the presented PFM inverter can be deemed as a sort of quantum resonant converter whose dc gain is quantized [19], [20]. Finally, a phase control [21] was presented for the purpose of wireless energy beamforming rather than wireless power regulation.

In some specific multiobjective WPT applications, the wireless energy selectivity can guarantee oriented power transmission to one specified receiver [5] or achieve multiplex power

---

Manuscript received June 23, 2019; revised September 9, 2019; accepted October 31, 2019. Date of publication November 10, 2019; date of current version February 20, 2020. This work was supported by the Hong Kong Research Grants Council, Hong Kong Special Administrative Region, China under Project 17204317. Recommended for publication by Associate Editor J. Itoh. *(Corresponding author: K. T. Chau.)*

W. Liu, K. T. Chau, W. Han, X. Tian, and W. H. Lam are with the Department of Electrical and Electronic Engineering, The University of Hong Kong, Hong Kong (e-mail: liuwei@eee.hku.hk; ktchau@eee.hku.hk; weihan@eee.hku.hk; xytian@eee.hku.hk; whlam@eee.hku.hk).

C. H. T. Lee is with the School of Electrical and Electronic Engineering, Nanyang Technological University, Singapore 639798 (e-mail: chtlee@ntu.edu.sg).

Color versions of one or more of the figures in this article are available online at http://ieeexplore.ieee.org.

Digital Object Identifier 10.1109/TPEL.2019.2952573

distributions among multireceivers [6]. Also, the wireless energy security via chaotic encryption [7] should be concerned and considered as one of the key factors in future practical implementations of the WPT technology, especially in multiobjective WPT applications. In fact, the selective WPT is realized by regularly modulating the operating frequency according to the targeted loads, while the energy-encrypted WPT is by chaotically modulating the operating frequency according to the security keys. Furthermore, the development of enhancement-mode gallium nitride (GaN) power devices [22], [23] will promisingly contribute to a significant advancement in both the conventional and emerging WPT-based areas.

In order to fulfill the practical requirements in various WPT applications, a full-range soft-switching PFM technology with wireless energy controllability, selectivity, and security is newly proposed and experimentally evaluated in this article. It can availably suppress the switching frequency and losses while maintaining the full-range soft-switching state, thus improving the system efficiency with insignificant output fluctuations.

Section II will discuss the proposed soft-switching PFM-WPT system and its operating principle. Section III will present a two-dimensional (2-D) chaotic frequency-and-duration encryption (FDE) to improve the wireless energy security. In Section IV, a full-range soft-switching PFM technology will be proposed and introduced to suppress the power losses and improve the system efficiency. In Section V, both simulation and experimental results will be given to verify the feasibility of proposed full-range soft-switching PFM-WPT scheme. A conclusion will be drawn in Section VI.

II. PFM WIRELESS ENERGY SYSTEM

A. PFM-WPT

The proposed soft-switching PFM-WPT system is depicted in Fig. 1. The whole selective or energy-encrypted WPT system mainly comprises one GaN full-bridge inverter, one transmitter, and multiple receivers including the authorized and unauthorized ones. According to the practical requests and load characteristics in terms of the frequency, duration, and wireless power-on-demand, the proposed PFM technology can be directly applied in various conventional and emerging WPT applications, in which the full-range soft-switching operation can be readily achieved without using any extra auxiliary circuits and power semiconductor components. Meanwhile, the full-range soft-switching PFM technology is competent to implement both the wireless power regulation and selective or energy-encrypted wireless power transmission. Unfortunately, the conventional PSC will deteriorate the soft-switching state once activating wireless power regulation. Thus, the involved inverter using the PSC inevitably suffers from degraded performance due to the high-frequency hard switching. In contrast, the proposed PFM-WPT scheme possesses the key merits of switching frequency reduction, switching loss suppression, full-range soft-switching operation and thus system efficiency improvement while maintaining good wireless energy controllability, selectivity, and security.

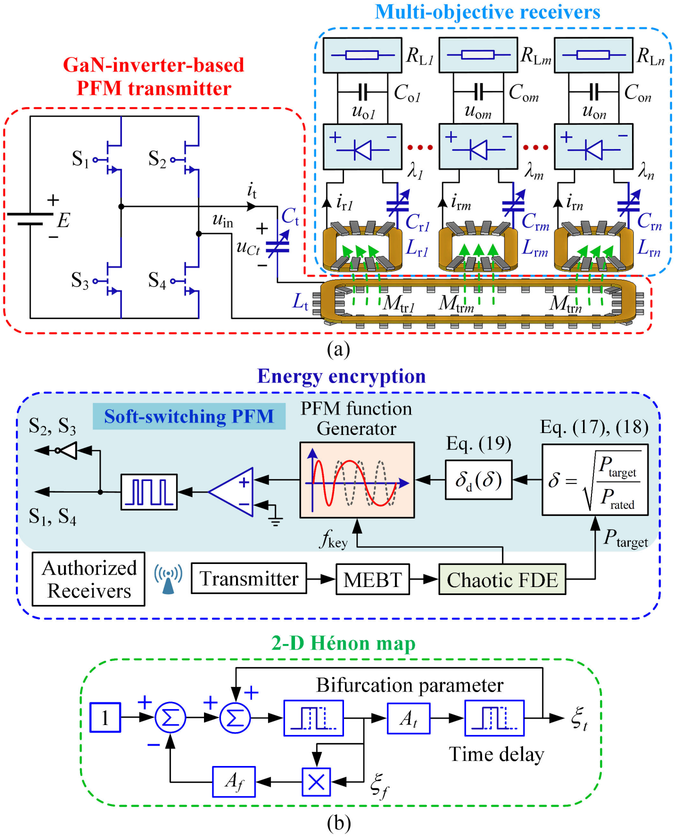

Fig. 1. Multiobjective GaN-inverter-based WPT system using proposed soft-switching PFM with controllability, selectivity and security. (a) Topology. (b) Soft-switching PFM and 2-D chaotic energy encryption.

Besides, Fig. 1(b) also illustrates the principle of newly proposed PFM incorporating with the 2-D chaotic energy encryption. The energy-encrypted WPT can be essentially regarded as a kind of chaotically frequency-modulated selective WPT. The proposed full-range soft-switching PFM can readily be incorporated into the energy-encrypted WPT scheme, where it can encrypt the wireless energy transmitting to the targeted receivers by using the Hénon map to generate the 2-D chaotic security keys (f_{key}, t_{key}) of frequency and duration. The transmitted wireless power is accordingly controlled by regulating the control objectives of proportion factor δ and thus duty ratio δ_d based on practical power-on-demand. A module of the PFM function generator will generate a fixed or chaotic PFM sine wave for the realization of the selective or energy-encrypted WPT, respectively. Via a zero-crossing comparator, the desired PFM gate signals are subsequently offered for power switches in the GaN inverter. For the wireless energy security, the maximum efficiency band tracking (MEBT) acts as a way to identify and detour the unsecure operating frequency where the energy theft happens.

B. Transient-State Analysis

In Fig. 1, L_t, R_t, C_t, i_t, u_{Ct}, L_{rk}, R_{rk}, C_{rk}, i_{rk}, and u_{Crk} $(k \in \mathbb{Z}^+)$ with subscripts *t* and *r* denote the resonant coil inductances, coil internal resistances, matched capacitances, *k*th

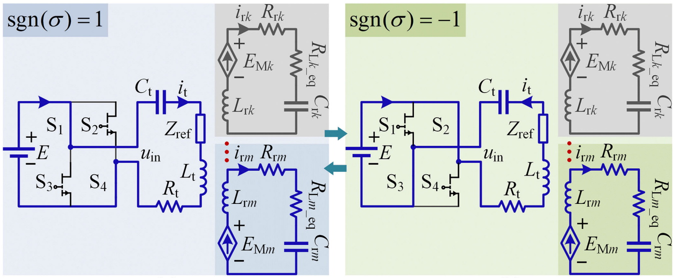

(a) (b)

Fig. 2. Operating modes of proposed PFM-WPT system. (a) Mode 1. (b) Mode 2.

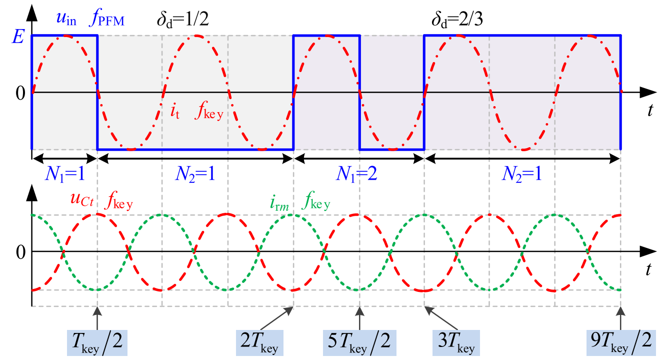

Fig. 3. Theoretical waveforms of proposed soft-switching PFM-WPT.

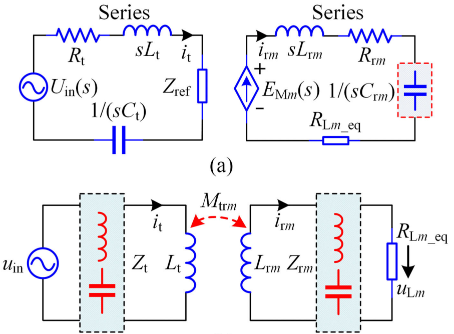

(a)

(b)

Fig. 4. Equivalent circuits. (a) Exemplified SS topology in the complex frequency domain. (b) Multitopological compensation networks.

resonant currents and resonant voltages of the transmitter and receiver circuits, respectively. Besides, λ_k is the number of the kth receivers, and M_{trk} is the mutual inductance between the transmitter and kth receiver coils. For illustration, L_{rm} $(k = m)$ denotes the mth receiver coil inductance. To commence with theoretical analysis, following assumptions are made:

1) symbol σ represents the positive or negative polarity of dc power source actually conducted via the inverter;
2) $u_{Ct}(0\_)$ denotes the initial voltage through C_t at the beginning of each switching period;
3) the mth receivers are specified to pick up wireless energy from the proposed PFM-WPT system, while the kth ($k{\neq}m$) ones are not.

The proposed soft-switching PFM-WPT operation can fall into the following two modes, as illustrated in Fig. 2, and each mode involves two stages.

1) Mode 1. Positive PFM Half-Cycle: The proposed PFM involves two optimal modulated frequencies of $f_{\text{key}}/(2n \pm 1)$ $(n = 1$ in Fig. 3), as derived in Appendix A. The dc power source is always positively connected to the transmitter circuit via the inverter, thus there is $\sigma = 1$. Its equivalent circuits and theoretical waveforms are depicted in Figs. 2(a) and 3, respectively. Denotation E_{Mk} is the induced electromotive force; $R_{Lk\_\text{eq}} = 8R_{Lk}/\pi^2$ is the equivalent ac resistance of the dc load R_{Lk}; and $T_{\text{key}} = 1/f_{\text{key}}$.

Stage 1 [0, T_{key}/2], [2T_{key}, 5T_{key}/2]: The involved modulated frequency is f_{key}. Switches S$_1$ and S$_4$ are turned ON while S$_2$ and S$_3$ are OFF so that the positive half-cycle resonance of L_t and C_t occurs. Fig. 4(a) shows the equivalent circuits of a series-to-series WPT topology in Fig. 1. Such a basic WPT topology can be promisingly extended to incorporate with other complex compensation networks, as shown in Fig. 4(b). According to these equivalent circuits, the key operating parameters in the complex frequency domain are expressed as

$$\begin{cases} i_t(s) = \frac{\mathrm{sgn}(\sigma)(E/s - u_{Ct}(0_-)/s)}{Z_{\text{ref}}+R_t+sL_t+1/(C_t s)} \\ u_{Ct}(s) = \mathrm{sgn}(\sigma)\left[\frac{E}{s} - \frac{u_{Ct}(0_-)}{s}\right] \frac{1/(C_t s)}{Z_{\text{ref}}+R_t+sL_t+1/(C_t s)} \end{cases} \tag{1}$$

where Z_{ref} is the total reflected impedance. After the inverse Laplace transform, (1) can be solved as

$$\begin{cases} i_t(t) = \mathrm{sgn}(\sigma)\frac{E-u_{Ct}(0_-)}{\omega_{\text{key}}L_t} e^{-\alpha t}\sin\left(\sqrt{1-(\alpha/\omega_{\text{key}})^2}\,\omega_{\text{key}}t\right) \\ u_{Ct}(t) = \mathrm{sgn}(\sigma)\Big[E - [E-u_{Ct}(0_-)]\,e^{-\alpha t} \\ \qquad \times \cos\left(\sqrt{1-(\alpha/\omega_{\text{key}})^2}\,\omega_{\text{key}}t\right)\Big] \end{cases} \tag{2}$$

where $\alpha = [(\omega_{\text{key}}M_{trm})^2/(R_{rm}+R_{Lm\_\text{eq}})+R_t]/(2L_t)$.

Stage 2 [3T_{key}, 9T_{key}/2]: The involved modulated frequency is f_{key}/3, and all the states of switches S$_1$–S$_4$ keep constant so that both the positive and negative half-cycle resonances of L_t and C_t occur, as shown in Fig. 3. Similarly, the key operating parameters can also be expressed as (2).

2) Mode 2. Negative PFM Half-Cycle: Since the dc power source is changed to negatively connect to the transmitter circuit via the inverter, there is $\sigma = -1$, and its equivalent circuits are depicted in Fig. 2(b).

Stage 1 [5T_{key}/2, 3T_{key}]: The involved frequency is modulated at f_{key}. The switches S$_2$ and S$_3$ are turned ON while S$_1$ and S$_4$ are OFF so that the negative half-cycle resonance of L_t and C_t occurs, as shown in Fig. 3. Both the corresponding analysis and expressions are the same as Stage 1 in Mode 1.

Stage 2 [T_{key}/2, 2T_{key}]: The involved frequency is modulated at f_{key}/3, and all the states of switches S$_1$–S$_4$ keep constant so that both the positive and negative half-cycle resonances of L_t and C_t occur, as shown in Fig. 3. Both the corresponding analysis and expressions are the same as Stage 2 in Mode 1.

Under the PSC-WPT, wireless power control is realized by regulating the duty ratio of directly or inversely conducting the dc power source for energizing the transmitter during each resonant half-cycle, but inevitably causing the high-frequency hard-switching losses and reducing the system efficiency.

Contrastively, it can be observed from Fig. 3 that all the switches could be turned ON or OFF exactly at or slightly before the zero-crossing points of the transmitter current i_t. It guarantees the soft-switching operation [24] withstanding various potential displacement deviations. This proposed PFM mechanism will effectively suppress the switching frequency and switching losses while retaining full-range soft-switching operation, thus improving the system efficiency during wireless power adjustment.

During each reduced-frequency switching point modulated at $f_{\text{key}}/(2n \pm 1)$ $(n > 1)$, there is a medium oscillation amplitude of the transmitter resonant voltage calculated as

$$u_{Ct\_\text{medium}} = E - [E - u_{Ct}(0_-)]\, e^{-n_{\text{sw}}\alpha T_{\text{key}}/2}(-1)^{n_{\text{sw}}} \quad (3)$$

where $n_{\text{sw}} = 2n \pm 1$, and $u_{Ct}(0\_) = -|u_{Ct\_\text{medium}}|$ when the modulated input voltage u_{in} has a symmetrical center in a whole PFM period. The fluctuations of transmitter resonant current and voltage can be calculated as

$$\begin{cases} \Delta i_{t\_\max} = \frac{[E - u_{Ct}(0_-)]}{\omega_{\text{key}} L_t}\left(e^{-\alpha T_{\text{key}}/4} - e^{-(2n_{\text{sw}}-1)\alpha T_{\text{key}}/4}\right) \\ \Delta u_{Ct\_\max} = [E - u_{Ct}(0_-)]\left(e^{-\alpha T_{\text{key}}/2} - e^{-(n_{\text{sw}}-1/2)\alpha T_{\text{key}}}\right). \end{cases} \quad (4)$$

According to (4), although the exponential decays may not be negligible in a whole PFM period, the proposed soft-switching PFM technology can still keep a good tolerance to such exponential decays to implement the MRC-based WPT.

C. Steady-State Analysis

The inverter square-wave output, which presents an odd function characteristic, can be expressed in Fourier series

$$u_{\text{in\_PSC}}(t) = \frac{4E}{n_F \pi} \cdot \sum_{n_F=1}^{\infty} \sin(n_F \pi/2) \times \sin(n_F D\pi) \sin(n_F \omega_{\text{key}} t) \quad (5)$$

where D is the duty ratio – a control objective of the PSC. It contains only the fundamental and the odd-order $(2n_F - 1)$th harmonics, whereas all the even-order $2n_F$th harmonics and the subharmonics are zero. In the proposed PFM, the equivalent root-mean-square (rms) value $U_{\text{in\_PFM}}$ of u_{in} can be derived as

$$U_{\text{in\_PFM}} = \frac{2\sqrt{2}E}{\pi\left[(2n-1)\,\delta_d + (2n+1)\,(1-\delta_d)\right]} = \delta U_{\text{in}} \quad (6)$$

where the duty ratio δ_d is a ratio of the number N_1 of the involved high-frequency switching half-cycles to the number $(N_1 + N_2)$ of the total modulated switching half-cycles as shown in Fig. 3; δ is a proportion factor; and $U_{\text{in}} = 2\sqrt{2}E/\pi$. As a control objective of the PFM, the proportion factor δ can be flexibly controlled by regulating the duty ratio δ_d, thus achieving wireless energy controllability.

By applying the steady-state first harmonic analysis, the necessary expressions of the proposed PFM-WPT are listed in Table I, where cosφ is the power factor. Accordingly, the general equation can be expressed as

TABLE I
STEADY-STATE ANALYSIS OF PROPOSED PFM-WPT SYSTEM

Parameters	Expressions of proposed PFM-WPT
Transmitter impedance Z_{t}	$Z_{\text{t}} = R_{\text{t}} + j\omega_{\text{key}}L_{\text{t}} + 1/(j\omega_{\text{key}}C_{\text{t}})$
Receiver impedance $Z_{\text{r}k}$	$Z_{\text{r}k} = R_{\text{L}k\_\text{eq}} + R_{\text{r}k} + j\omega_{\text{key}}L_{\text{r}k} + 1/(j\omega_{\text{key}}C_{\text{r}k})$
Reflected impedance $Z_{\text{ref}k}$	$Z_{\text{ref}k} = \frac{(\omega_{\text{key}}M_{\text{tr}k})^2}{Z_{\text{r}k}},\ Z_{\text{ref}m} = \frac{(\omega_{\text{key}}M_{\text{tr}m})^2}{R_{\text{L}m\_\text{eq}} + R_{\text{r}m}}$
Input impedance Z_{in}	$Z_{\text{in}} = Z_{\text{t}} + \sum_{k=1,\, k\neq m}^{n}(\lambda_k Z_{\text{ref}k}) + \lambda_m \frac{(\omega_{\text{key}}M_{\text{tr}m})^2}{R_{\text{L}m\_\text{eq}} + R_{\text{r}m}}$
Transmitter and receiver currents I_{t} and $I_{\text{r}k}$	$I_{\text{t}} = \delta U_{\text{in}}/Z_{\text{in}},\ I_{\text{r}k} = (-j\omega_{\text{key}}M_{\text{tr}k}I_{\text{t}})/Z_{\text{r}k}$
Transmitter voltage U_{Ct}	$U_{Ct} = I_{\text{t}}/(j\omega_{\text{key}}C_{\text{t}}) = \delta U_{\text{in}}/(j\omega_{\text{key}}C_{\text{t}}Z_{\text{in}})$
Receiver voltage U_{Crk}	$U_{Crk} = \frac{-M_{\text{tr}k}I_{\text{t}}}{C_{\text{r}k}Z_{\text{r}k}},\ U_{Crm} = \frac{-M_{\text{tr}m}I_{\text{t}}}{C_{\text{r}m}(R_{\text{L}m\_\text{eq}} + R_{\text{r}m})}$
Input and output powers P_{in} and $P_{\text{out}k}$	$P_{\text{in}} = (\delta U_{\text{in}})^2 \cos\varphi/\lvert Z_{\text{in}}\rvert,\ P_{\text{out}k} = \lvert I_{\text{r}k}\rvert^2 R_{\text{L}k\_\text{eq}}$
Transmission efficiency η_k	$\eta_k = \frac{\lambda_k R_{\text{L}k\_\text{eq}}(\omega_{\text{key}}M_{\text{tr}k})^2}{\lvert Z_{\text{r}k}\rvert^2\left(\Re\left(\sum_{k=1}^{n}\lambda_k Z_{\text{ref}k}\right) + R_{\text{t}}\right)}$

$$\begin{bmatrix} Z_t & Z_{tr1}\lambda_1 & \cdots & Z_{trm}\lambda_m & \cdots & Z_{trn}\lambda_n \\ Z_{tr1} & Z_{r1} & \cdots & 0 & \cdots & 0 \\ \vdots & \vdots & \ddots & \vdots & \ddots & \vdots \\ Z_{trm} & 0 & \cdots & Z_{rm} & \cdots & 0 \\ \vdots & \vdots & \ddots & \vdots & \ddots & \vdots \\ Z_{trn} & 0 & \cdots & 0 & \cdots & Z_{rn} \end{bmatrix} \begin{bmatrix} I_t \\ I_{r1} \\ \vdots \\ I_{rm} \\ \vdots \\ I_{rn} \end{bmatrix} = \begin{bmatrix} \delta U_{\text{in}} \\ 0 \\ \vdots \\ 0 \\ \vdots \\ 0 \end{bmatrix} \quad (7)$$

where $Z_{trk} = j\omega_{\text{key}}M_{trk}$; Z_t and Z_{rk} are listed in Table I. From (7), it yields

$$\delta U_{\text{in}} = Z_t I_t + \sum_{k=1}^{n}(\lambda_k Z_{trk} I_{rk}) \quad (8)$$

$$Z_{trk} I_t + Z_{rk} I_{rk} = 0. \quad (9)$$

Thus, the receiver current can be derived as

$$I_{rk} = -Z_{trk} I_t / Z_{rk} = -j\omega_{\text{key}} M_{trk} I_t / Z_{rk}. \quad (10)$$

From (8) and (10), the input impedance can be expressed as

$$Z_{\text{in}} = \delta U_{\text{in}}/I_t = Z_t + \sum_{k=1}^{n}\left(-\lambda_k Z_{trk}^2/Z_{rk}\right) = Z_t + \sum_{k=1}^{n}\left[\lambda_k(\omega_{\text{key}}M_{trk})^2/Z_{rk}\right] = Z_t + \sum_{k=1}^{n}(\lambda_k Z_{\text{ref}k}). \quad (11)$$

The reflected impedances of $Z_{\text{ref}k}$ and $Z_{\text{ref}m}$ can be written as

$$Z_{\text{ref}k} = (\omega_{\text{key}} M_{trk})^2 / Z_{rk} \quad (12)$$

$$Z_{\text{ref}m} = (\omega_{\text{key}} M_{trm})^2 / (R_{Lm\_\text{eq}} + R_{rm}). \quad (13)$$

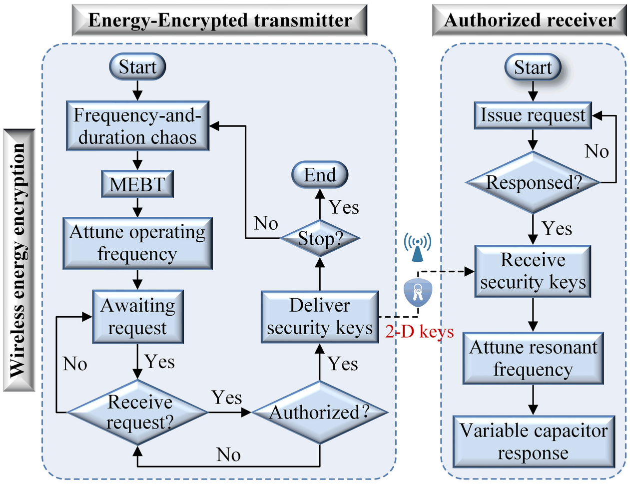

Fig. 5. 2-D chaotic FDE scheme.

Finally, the transmission efficiency can be calculated as (14) shown at the bottom of this page, where $\Re(\cdot)$ and $\Im(\cdot)$ denote the real part and the imaginary part, respectively.

In the multiobjective PFM-WPT, both the primary and selected secondary circuits operate at the same resonant angular frequency as given by $\omega_{\text{key}} = 1/\sqrt{L_t C_t} = 1/\sqrt{L_{rm} C_{rm}}$, which is an odd multiple of the modulated reduced angular frequency $\omega_{\text{key}}/(2n \pm 1)$. Also, the transient and steady-state analyses can be interrelated by $|u_{Ct}(0_-)| = \sqrt{2} U_{Ct} = \sqrt{2} I_t/(\omega_{\text{key}} C_t)$ when the modulated input voltage exists a symmetrical center in a whole PFM period.

III. 2-D FREQUENCY AND DURATION ENCRYPTION

Essentially as a specific selective WPT, energy encryption mainly relies on the frequency sensitivity of MRC-based WPT systems. The 2-D chaotic energy encryption scheme is depicted in Fig. 5, where the energy-encrypted transmitter generates a 2-D chaotic sequence – the security keys (f_{key}, t_{key}), where t_{key} is the active duration of each encrypted f_{key}. The principle of the MEBT is based on the actual system efficiency from the transmitter to the selected receivers. Once the energy theft or leakage happens due to unselected receivers, the system efficiency will be significantly reduced. Hence, the energy theft and the unsecure operating frequency will be both readily identified. Consequently, the MEBT will detour this unsecure frequency and dynamically reconstruct a new optimal modulated frequency band to prevent the wireless energy leakage, hence maximizing the transmission efficiency. As depicted in Fig. 5, the security keys are delivered by data interaction based on wireless communication, such as Bluetooth communication, which is independent of the WPT. Considering the risks of pilfering wireless data and energy by illegal receivers, the out-of-band digital information interaction is preferred for the identification and authentication of legal receivers. With knowledge of the security keys via wireless communication, both the transmitter and authorized receivers will proactively and simultaneously attune their resonant frequencies to the 2-D chaotic security keys for dynamical energy encryption and decryption, respectively. By this way, only the authorized receiver can successfully decrypt and pick up the encoded energy packages from the chaotic PFM-WPT system. Due to the lack of security keys, the unauthorized ones can steal only an insignificant level of wireless energy.

The 2-D FDE algorithm plays an important role in ensuring wireless energy security. In Fig. 1(b), the Hénon map [25] is used to generate a discrete-time chaotic series as given by

$$\begin{cases} \xi_{f\_i+1} = \xi_{t\_i} + 1 - A_f \xi_{f\_i}^2 \\ \xi_{t\_i+1} = A_t \xi_{f\_i} \end{cases}, \quad A_f \in [1.0,\ 1.5],\ A_t = 0.3 \tag{15}$$

where ξ_{f_i} and ξ_{t_i} denote the chaotic sequences of the encrypted frequency and its duration, respectively, and A_f and A_t are the bifurcation parameters. Subsequently, the discrete 2-D chaotic FDE sequences are generated as $(\gamma_i \omega_0,\ \beta_i t_0)$, where $\gamma_i = a_\gamma + b_\gamma \xi_f$ and $\beta_i = a_\beta + b_\beta \xi_t$. Generally, ω_0 and t_0 can be designed based on the power level, transfer distance, and security requirements. Accordingly, both the transmitter and authorized receiver adjust their matched capacitors as

$$C_x \left(\sum_{q=1}^{q=i} \left(a_\beta + b_\beta \xi_{t\_i} \right) t_0 \right) = \frac{1}{\left(a_\gamma + b_\gamma \xi_{f\_i} \right)^2} \frac{1}{\omega_0^2 L_x} \tag{16}$$

where the subscript *x* of C_x and L_x is t or r*m* denoting the transmitter or authorized receiver. Besides, $0 < 1.5 b_\gamma < a_\gamma, 0 < 0.4 b_\beta < a_\beta$, and $A_f = 1.4$ is selected [25] to produce the desired random-like but bounded security series $(\xi_f,\ \xi_t)$. Consequently, the frequency and its duration can be chaotically modulated and thus encrypted, and the encoded energy package can be decoded and picked up only by the authorized receiver.

Considering the wireless energy security, the regulating range of the matched capacitor requires to reach from the minimum capacitance to around four or nine multiples larger. Correspondingly, its frequency variation range can reach from the lowest frequency to two or three times higher, such as varying from 75 to 150 kHz or 225 kHz. For adjusting the matched capacitor in real

$$\begin{aligned} \eta_k &= \frac{P_{\text{out}k}}{P_{\text{in}}} = \frac{\lambda_k |I_{rk}|^2 R_{Lk\_\text{eq}}}{\delta U_{\text{in}} |I_t| \cdot \Re(Z_{\text{in}}) / |Z_{\text{in}}|} = \frac{\lambda_k R_{Lk\_\text{eq}} |-j\omega_{\text{key}} M_{trk} I_t / Z_{rk}|^2}{|I_t Z_{\text{in}}| \cdot |I_t| \cdot \Re(Z_{\text{in}}) / |Z_{\text{in}}|} = \frac{\lambda_k R_{Lk\_\text{eq}} (\omega_{\text{key}} M_{trk})^2}{\Re(Z_{\text{in}}) |Z_{rk}|^2} \\ &= \frac{\lambda_k R_{Lk\_\text{eq}} (\omega_{\text{key}} M_{trk})^2}{|Z_{rk}|^2 \Re \left[\Re\left(\sum\limits_{k=1}^{n} \lambda_k Z_{\text{ref}k} \right) + j \cdot \Im \left(\sum\limits_{k=1}^{n} \lambda_k Z_{\text{ref}k} \right) + R_t + j\omega_{\text{key}} L_t + \frac{1}{j\omega_{\text{key}} C_t} \right]} = \frac{\lambda_k R_{Lk\_\text{eq}} (\omega_{\text{key}} M_{trk})^2}{|Z_{rk}|^2 \left[\Re\left(\sum\limits_{k=1}^{n} \lambda_k Z_{\text{ref}k} \right) + R_t \right]} \end{aligned} \tag{14}$$

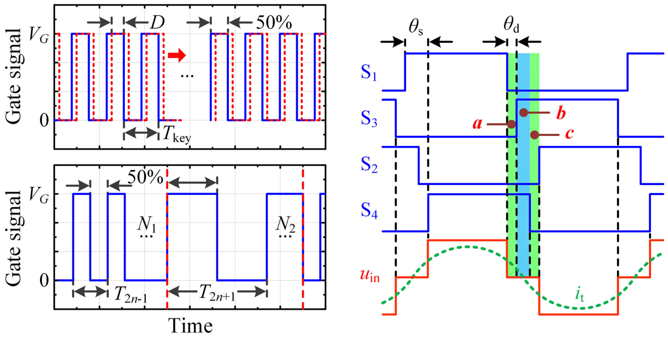

(a) (b)

Fig. 6. Alternative control methods. (a) Gate signals of conventional PSC (top) and proposed PFM (bottom). (b) Principle of the PSC.

time, the scheme of switched-capacitor arrays, which comprise multiple switches and capacitors is adopted in the proposed PFM-WPT system. It is an effective way to dynamically adjust the matched capacitor according to the 2-D chaotic security keys. A larger adjustment range of capacitors will contribute to a wider range of frequency variation, which can be achieved by increasing the number of switched capacitors. Such a wider frequency variation range will promisingly improve the energy security performance with more selections of modulated frequencies.

IV. SOFT-SWITCHING PFM

A. Oscillation Frequency Invariance

In the selective WPT, the system operates at the resonant frequency of the mth selected receivers. According to Table I, there are $Z_{rk} \gg Z_{rm}$ and $Z_{\text{ref}k} \ll Z_{\text{ref}m} (k \neq m)$, where $Z_{\text{ref}k}$ can be regarded as zero. Hence, the system oscillation frequency is dominantly determined by the selected receivers rather than the unselected ones. Generally, the multiobjective WPT system operates within a loosely coupling regime. By substituting the actual parameters, the deviation coefficient can be calculated as $(\alpha/\omega_{\text{key}})^2 = 4.972 \times 10^{-3} \simeq 0 \ll 1$. Furthermore, this coefficient will be further reduced with a weaker magnetic coupling due to misalignment or longer transfer distance. The frequency deviation factor is $\sqrt{1-(\alpha/\omega_{\text{key}})^2}=0.9975\simeq 1$. The system resonant frequency of the WPT input impedance can be revealed by the resonant angular frequency in the transmitter side. Thus, the actual transmitter's resonant angular frequency can be further derived as $\omega_t = \omega_{\text{key}}\sqrt{1-(\alpha/\omega_{\text{key}})^2} \simeq \omega_{\text{key}}$.

The system oscillation frequency invariance is proved in detail in Appendix A. It indicates that the oscillation frequency can keep constant in the proposed PFM-WPT system even variably modulated at the reduced switching frequencies. As a result, this oscillation frequency invariance successfully contributes to the proposed full-range soft-switching PFM-WPT operation regularly or chaotically modulated between two optimal switching frequencies of $f_{\text{key}}/(2n \pm 1)$.

B. Full-Range Soft-Switching PFM

Two alternative control methods of the proposed PFM and the PSC are illustrated in Fig. 6, in which the switching frequency is effectively reduced by applying the proposed PFM while it retains constant by using the PSC. In Fig. 6(b), θ_d and θ_s are the angles of the dead zone and shifted phase, respectively. During the shifted phase of the PSC, it can theoretically fall into three transition stages ***a***, ***b***, and ***c***, where stages ***a*** and ***c*** are the dead-zone stages while stage ***b*** is the freewheeling stage, and the deterioration of high-frequency soft switching will induce more switching losses.

In the full range of wireless power adjustment, the transmitter resonant current i_t can be successfully energized by the frequency-modulated input voltage u_{in} under the proposed PFM, as shown in Fig. 3. Thus, the ZVS is reliably ensured by slight frequency or compensation deviation for producing a tiny reactance. The soft-switching PFM can effectively reduce the switching frequency and power losses, hence improving the system efficiency. Moreover, it is also promising and practically attractive for various WPT applications involving full-bridge or half-bridge inverters constructed by silicon-carbon (SiC) MOSFETs or silicon insulated gate bipolar translators. The proposed PFM is implemented by selecting two optimal fundamental or subharmonic frequencies of $f_{2n\pm1} = f_{\text{key}}/(2n \pm 1)$ and then regularly modulating between them. Nevertheless, the WPT frequency retains constant at f_{key}. The PFM-WPT system can generate two optimal receiver current vectors of $I_{2n\pm1} = I_{\text{rated}}/(2n \pm 1)$ and thus receiver power vectors of $P_{2n\pm1} = P_{\text{rated}}/(2n \pm 1)^2$, which can be modulated to composite arbitrary targeted vectors of output current or power.

The proposed soft-switching PFM can be competent for two control modes of wireless power P_{target} and wireless current I_{target}. Both control modes are interrelated by

$$P_{\text{target}} = \delta^2 P_{\text{rated}} = R_{Lm\_\text{eq}} I_{\text{target}}^2 \tag{17}$$

$$I_{\text{target}} = \delta I_{\text{rated}} = \frac{I_{\text{rated}}}{(2n-1)\,\delta_d + (2n+1)\,(1-\delta_d)}, \quad n \in \mathbb{Z}^+ \tag{18}$$

where P_{rated} and I_{rated} are the rated wireless output power and receiver current when modulating at the fixed f_{key}. According to Fig. 6(a), the duty ratio δ_d in the PFM can be predicted by

$$\delta_d = \frac{N_1}{N_1 + N_2} = \frac{(2n+1) - 1/\delta}{2}, \ (N_1, \ N_2 \in \mathbb{N}) \tag{19}$$

where N_1 and N_2 are the minimum half-cycle numbers of two optimal switching periods of $T_{2n\pm1}$, corresponding to two modulated frequencies of $f_{\text{key}}/(2n \pm 1)$. Also, N_1 and N_2 should be minimized to effectively suppress the modulated input fluctuations. Some soft-switching PFM examples are listed in Table II for illustration, where $n = 1$; T_{PFM} is the minimum PFM period and can be expressed as $T_{\text{PFM}} = (N_1 T_{2n-1} + N_2 T_{2n+1})/2$. The relevant results are derived in Appendix A. When the modulated input voltage has a symmetrical center, N_1 is an odd number while N_2 is an even number. The PSC and proposed PFM can use the control objectives of duty ratio D and proportion factor δ to realize wireless energy controllability, respectively, and they are interrelated by $\delta = \sin(D\pi)$ for outputting the same power.

TABLE II
SOFT-SWITCHING PFM EXAMPLES

δ_d	δ	T_{PFM}	Modulated input voltage u_{in} and current i_t	I_{target} (*pu*)	P_{target} (*pu*)
1	1	T_{key}	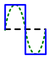	1	1
1/2	1/2	$2T_{key}$	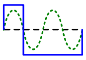	1/2	1/4
1/3	3/7	$7T_{key}$	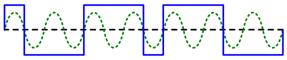	3/7	9/49
2/3	3/5	$5T_{key}$	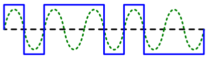	3/5	9/25
1/4	2/5	$5T_{key}$	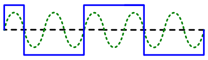	2/5	4/25
3/4	2/3	$3T_{key}$	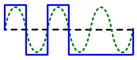	2/3	4/9

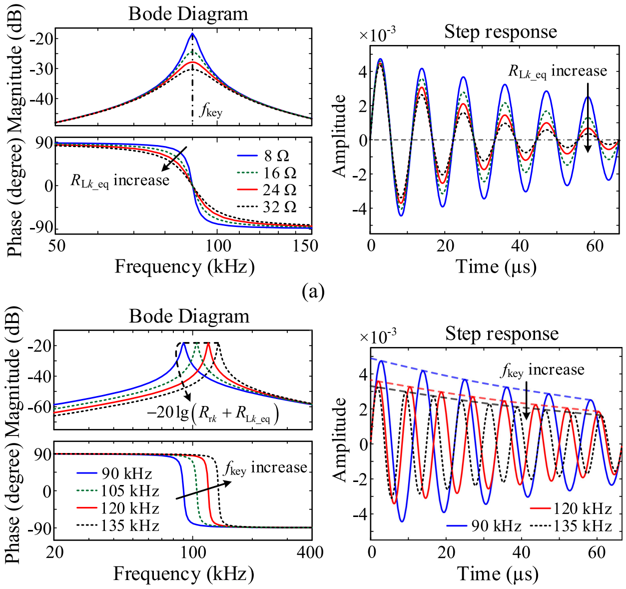

(a)

(b)

Fig. 7. Receiver circuit characteristics. (a) Bode plots and step responses versus loads. (b) Bode plots and step responses versus operating frequencies.

C. Output Fluctuation Assessment

To quantitatively assess the output fluctuations, a transfer function of the secondary equivalent circuit in Fig. 4(a) is established as

$$G_{rk}(s)=\frac{i_{rk}(s)}{E_{Mk}(s)}=\frac{C_{rk}s}{L_{rk}C_{rk}s^2+(R_{rk}+R_{Lk})\,C_{rk}s+1}. \tag{20}$$

Its steady-state gain can be derived as $K_{Gk}=0$ in the step response. According to (20), both the bode plots and step responses are elaborated in detail to evaluate the PFM-WPT output fluctuations at various conditions of loads and operating frequencies in Fig. 7. Both the low magnitudes in the bode plots and low amplitudes in the step responses can well verify the low steady-state and transient gains at the desired resonant frequency and thus insignificant output fluctuations. In Fig. 7(a), the low steady-state gains and transient output fluctuations can be further suppressed with the increasing loads at a fixed resonant frequency. With a fixed load, Fig. 7(b) indicates that the low steady-state gains may keep constant versus various operating frequencies, while the transient output fluctuations will become lower with the increasing operating frequencies. Thus, the larger load and the higher operating frequency will contribute to more insignificant output fluctuations. By modulating between two optimal frequencies and minimizing N_1 and N_2, the proposed PFM-WPT system can be effectively optimized to lower input fluctuations, which will further suppress output fluctuations.

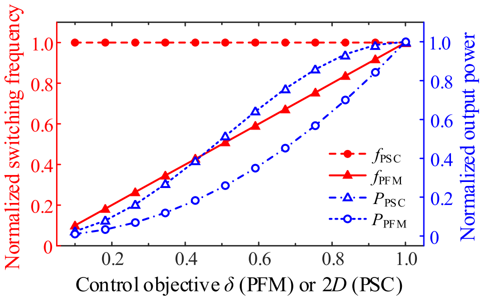

Fig. 8. Normalized average switching frequency and wireless power controllability under proposed soft-switching PFM and conventional PSC.

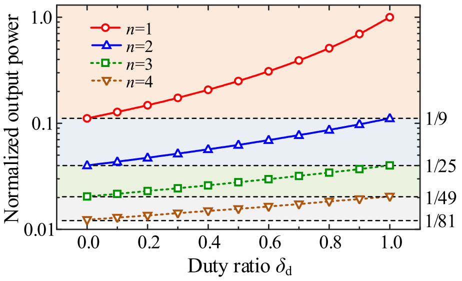

Fig. 9. Normalized output power versus duty ratio with different n under the PFM.

D. Controllability, Selectivity, and Security

To illustrate wireless energy controllability of the proposed soft-switching PFM, Fig. 8 shows the normalized output powers of P_{PFM} and P_{PSC} versus control objectives of δ $(0<\delta\leq 1)$ in the proposed PFM and D $(0<D\leq 50\%)$ in the PSC, respectively. In Fig. 8, the base value of the switching frequency is the selected frequency of 115.0 kHz for selective WPT, and that of the output power is 257.61 W. The two wireless output powers exhibit a monotonous increase with the increasing control objectives in the two abovementioned control methods. Fig. 8 also demonstrates that the normalized average switching frequency f_{PFM} of the PFM will monotonously reduce with the decreasing output power, much lower than the constant high switching frequency f_{PSC} of the PSC. It indicates that the proposed PFM can promisingly suppress the switching losses and thus improve the system efficiency. Under the PFM, Fig. 9 shows the trends of normalized output power versus the duty ratio with different n. The normalized power has the same base value of 257.61 W. The wireless power adjustment is continuous. In most scenarios, $n=1$ will satisfy the general requirements of power control. Nevertheless, a larger n can be chosen for controlling the lower

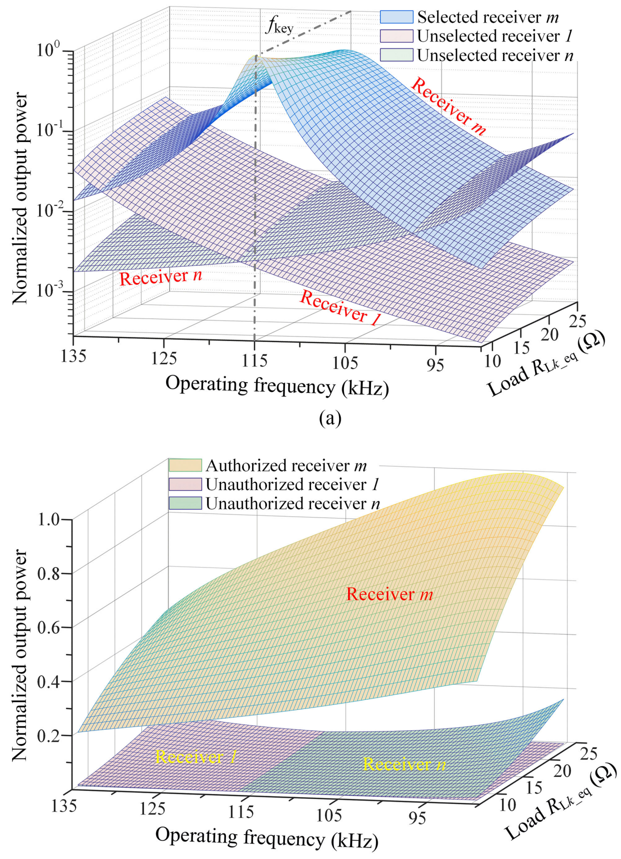

(a)

(b)

Fig. 10. Wireless power characteristics of proposed PFM-WPT system. (a) Selectivity. (b) Security.

power, and thus lower modulated frequencies of $f_{\mathrm{key}}/(2n \pm 1)$ will be involved. The average switching frequency will become lower, as indicated in Fig. 8. The system efficiency can be readily improved due to the full-range low-frequency soft-switching operation.

The wireless energy selectivity and security are demonstrated in Fig. 10(a) and (b), respectively, where the receiver m is selected or authorized to harvest the PFM wireless energy. In Fig. 10(a) and (b), their base values are 257.61 W and 604.27 W, respectively. Fig. 10(a) shows the normalized output powers of three receivers with respect to different loads and operating frequencies. By modulating f_{key} at the mth receiver's frequency, only the receiver m succeeds to pick up large wireless power, while the unselected receivers l and n can harvest only insignificant wireless power. The wireless energy security mainly relies on this selectivity characteristic with a chaotically encrypted PFM-WPT operation. In Fig. 10(b), the authorized receiver m can always successfully decrypt and harvest the encoded wireless energy packages, while the unauthorized ones fail to pick up energy due to the lack of security keys, which guarantees the wireless energy security in the chaotic PFM-WPT system.

E. Power Loss Discussion

Although the switching frequency is reduced by using the PFM, the PFM-WPT still resonates at the same innate frequency as the PSC-WPT. The same resonant parameters of both inductors and matched capacitors are used in the abovementioned two schemes. Generally, their parameter values and power losses may both affect the sizes of inductors and capacitors. Assuming that only the mth receivers are selected to harvest the wireless energy, the power losses of unselected receiver circuits are not considered during power loss calculation.

In the PFM-WPT, the input fluctuations and the total harmonic distortions (THDs) may not be neglected in the transmitter circuit, while they are insignificant in the receiver one. The transmitter inductor and capacitor losses should account for all the fundamental and harmonic (n_Fth) components, while the receiver ones need not to do so. Although the harmonic equivalent internal resistances may differ from the fundamental one, such differences are insignificant for the relatively low harmonic amplitudes. The transmitter inductor loss P_{Lt} and the receiver one P_{Lr} can be, respectively, calculated as

$$P_{Lt} = \sum_{n_F=1}^{\infty} \left(I_{t,n_F}^2 R_t \right) \tag{21}$$

$$P_{Lr} = \sum_{n_F=1}^{\infty} \left(\sum_{k=1}^{n} \left(\lambda_k I_{rk,n_F}^2 R_{rk} \right) \right) \simeq \lambda_m I_{rm,1}^2 R_{rm} \tag{22}$$

where denotations with the subscript n_F denote the n_Fth harmonic components. For example, I_{rk,n_F} is the n_Fth harmonic current of the kth receiver.

Due to better ac performance, the polyester film capacitors are chosen. Instead of the equivalent series resistances R_{t_ESR} and R_{rk_ESR}, the manufacturers usually provide their dissipation factors of $\tan\delta_t$ and $\tan\delta_{rk}$ for the transmitter and kth receiver capacitors, respectively. Considering the harmonic losses, the transmitter capacitor loss P_{Ct} and the receiver one P_{Cr} can be, respectively, expressed as

$$P_{Ct} = \sum_{n_F=1}^{\infty} \left(U_{Ct,n_F} I_{t,n_F} \tan\delta_t \right) = \sum_{n_F=1}^{\infty} \left(I_{t,n_F}^2 R_{t\_\mathrm{ESR}} \right) \tag{23}$$

$$P_{Cr} = \sum_{n_F=1}^{\infty} \left(\sum_{k=1}^{n} \left(\lambda_k U_{Crk,n_F} I_{rk,n_F} \tan\delta_{rk} \right) \right) \simeq \lambda_m U_{Crm,1} I_{rm,1} \tan\delta_{rm} = \lambda_m I_{rm,1}^2 R_{rm\_\mathrm{ESR}}. \tag{24}$$

Since the PSC-WPT is dominated by the fundamental component, all the power losses on inductors and capacitors only account for their fundamental losses [17]. As a result, the low harmonics will cause slightly higher losses on the transmitter inductor and capacitor in the PFM-WPT. Nevertheless, the fundamental losses still dominate the total inductor and capacitor losses. Considering the insignificant output fluctuations, the losses on the receiver inductor and capacitor keep approximately constant in the abovementioned two schemes. With only a slight increase in power losses, the sizes of both inductors and capacitors are nearly unaffected by using the proposed PFM technique.

The GaN switch has no intrinsic body diode. Within the dead zone, however, it can be modeled as a "body diode" with slightly higher forward voltage and no reverse recovery charge. It will

TABLE III
DESIGN SPECIFICATIONS AND PARAMETERS

Items	Value
Digital signal processer	TMS320F28335
GaN E-HEMT	GS66516B
Transmitter capacitance (C_{t})	2.1023~6.9063 nF
Transmitter coil inductance (L_{t})	573.08 μH
Transmitter coil turns (n_{t})	24
Transmitter coil internal resistance (R_{t})	0.29 Ω
Receiver capacitances ($C_{\mathrm{r}1}$, $C_{\mathrm{r}n}$)	3.4504, 11.450 nF
Receiver capacitance ($C_{\mathrm{r}m}$)	3.8987~7.8729 nF
Receiver coil inductances ($L_{\mathrm{r}1}$, $L_{\mathrm{r}m}$, $L_{\mathrm{r}n}$)	349.17, 356.50, 345.67 μH
Receiver coil turns ($n_{\mathrm{r}k}$)	30 (3 layers)
Receiver coil internal resistance ($R_{\mathrm{r}k}$)	0.18 Ω
Mutual inductances ($M_{\mathrm{tr}1}$, $M_{\mathrm{tr}m}$, $M_{\mathrm{tr}n}$)	28.55, 33.38, 27.42 μH
Load resistance ($R_{\mathrm{L}k}$)	10 Ω

lead to insignificant reverse conduction loss. The switch loss P_S comprises the switch conduction loss P_{con}, switching loss P_{sw} and diode loss P_{diode}. Under the PSC, the loss P_S can be expressed as

$$\begin{aligned} P_S &= P_{\text{con}} + P_{\text{sw}} + P_{\text{diode}} \\ &= 2I_{t,1}^2 R_{DS} + 4f_{\text{key}}\left(E_{\text{on}} + E_{\text{off}}\right) + P_{\text{diode}} \end{aligned} \tag{25}$$

where R_{DS} is the on-resistance and E_{on} or E_{off} is the switching energy during turn ON or turn OFF. The main part of power loss on switches is due to the high-frequency hard switching.

For full-range soft switching, only the conduction loss is considered [17] under the PFM. Thus, the loss P_S can be accordingly rewritten as

$$P_S = P_{\text{con}} + P_{\text{diode}} = 2\sum_{n_F=1}^{\infty}\left(I_{t,n_F}^2 R_{DS}\right) + P_{\text{diode}}. \tag{26}$$

Besides, the power loss on driving circuits is quite low as the PFM has a lower switching frequency than the PSC.

Meanwhile, the switching loss of SiC diodes is not considered. The diode bridge loss is simply the conduction loss caused by the diode forward voltage V_F as given by

$$P_D = \sum_{n_F=1}^{\infty}\left(\sum_{k=1}^{n}\left(2\lambda_k V_F I_{rk,n_F}\right)\right) \simeq 2\lambda_m V_F I_{rk,1}. \tag{27}$$

Finally, the PSC will lead to more switching loss as compared with the PFM. Such high-frequency hard-switching loss caused by the PSC will dominantly increase the overall system loss P_{total}. Thus, the overall loss using the PSC will become much larger than that using the PFM, thus deteriorating the system performance.

V. RESULTS AND VERIFICATIONS

To illustrate the feasibility of the proposed soft-switching PFM-WPT system, both computational simulation and practical experimentation are performed. The design specifications and parameters are listed in Table III. The GaN inverter consists of two half bridges – GSP65R13HB, which are populated with GaN enhancement-mode high-electron-mobility transistors of GS66516B. The specification of Litz wire is 250 × 0.10 mm.

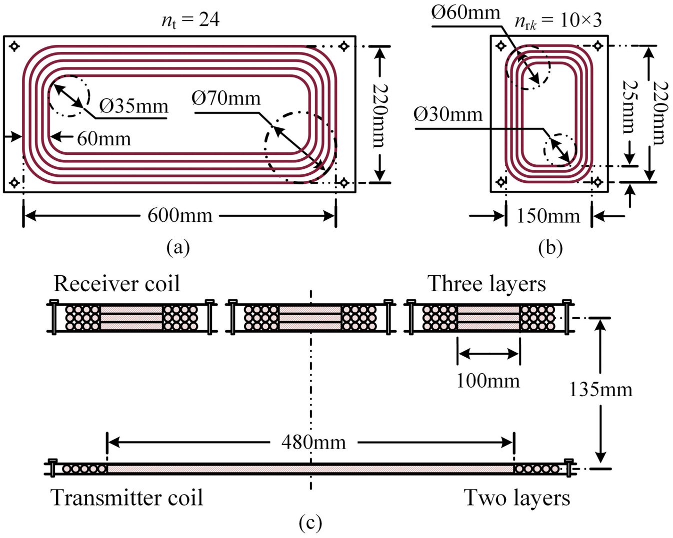

Fig. 11. Geometries of transmitter and receiver coils. (a) Transmitter coil. (b) Receiver coil. (c) Displacement among transmitter and receiver coils.

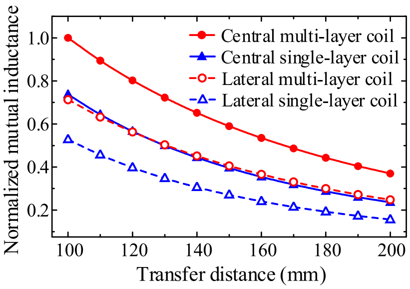

Fig. 12. Normalized mutual inductances versus transfer distance.

A. Simulation Results

Detailed geometries with dimensions of the transmitter and receiver coils are depicted in Fig. 11, where each receiver can be separately assigned to harvest wireless energy, and the transfer distance is 135 mm. A multilayer configuration is adopted in the receiver coils for enhancing the magnetic coupling and improving the system efficiency. By using the finite element analysis (FEA), the proposed PFM-WPT system is simulated based on the WPT coil geometries in Fig. 11. The FEA results of the normalized mutual inductances versus different transfer distances are plotted in Fig. 12. The multilayer configuration can effectively enhance the mutual inductances for both the central and lateral receiver coils as compared with the single-layer counterparts.

The FEA results of magnetic field distributions are shown in Fig. 13, where the magnetic flux pipe can be effectively built up in the proposed PFM-WPT system. As shown in Fig. 13(a), the vast majority of magnetic flux lines are bundled up through the central selected or authorized receiver, and only insignificant ones are dispersed. Also, the central selected or authorized receiver induces much higher current densities than the others do, thus harvesting nearly all the wireless energy. Along the vertical plane, the contour plots of the magnetic flux densities

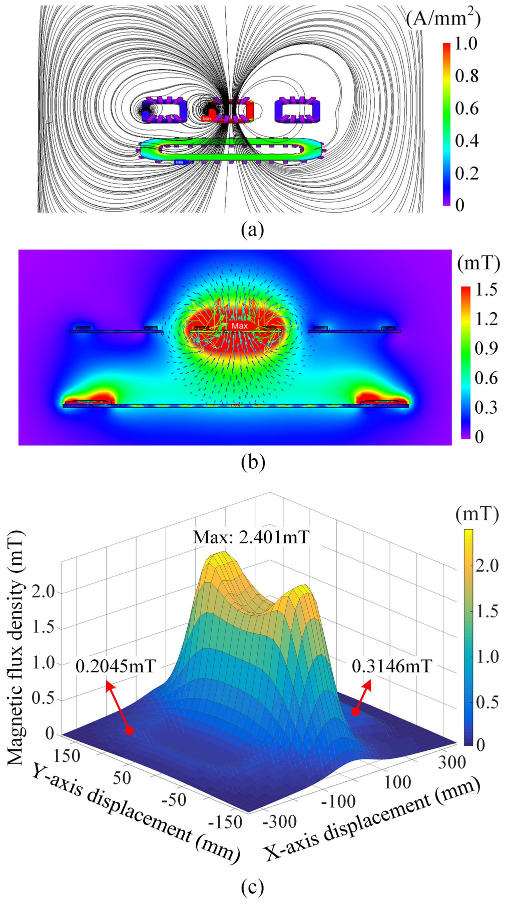

Fig. 13. Magnetic field distributions. (a) Flux lines and current densities. (b) Flux densities along the vertical plane. (c) 3-D flux densities along the parallel plane.

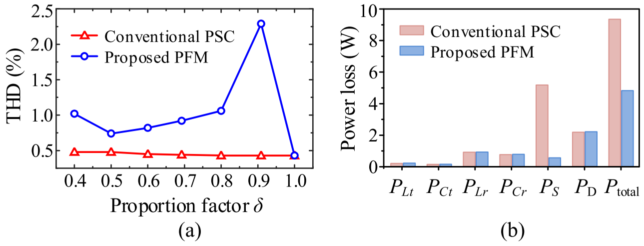

Fig. 14. Characteristic comparisons of the proposed PFM and the PSC. (a) THDs of authorized receiver current. (b) Power losses.

in Fig. 13(b) show that the magnetic fields around the central selected or authorized receiver are far stronger than those around the others. Along the parallel plan, Fig. 13(c) shows that the 3-D saddle-shaped magnetic flux densities under the central selected or authorized receiver can reach 2.401 mT, much larger than those of 0.2045 mT and 0.3146 mT under the other receivers. The magnetic field distributions indicate that only the selected or authorized receiver can pick up much larger wireless energy, while the unselected or unauthorized receivers can steal only insignificant wireless energy. Thus, the proposed PFM-WPT system exhibits good wireless energy selectivity and security.

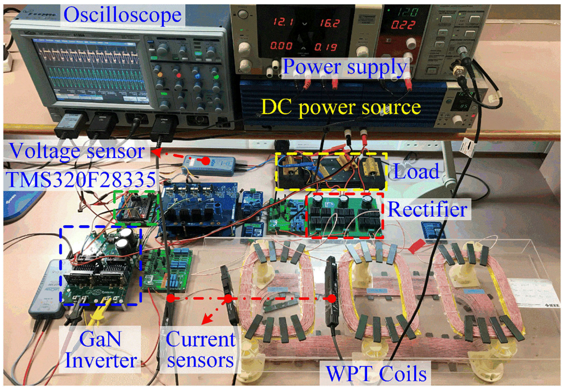

Fig. 15. Experimental setup.

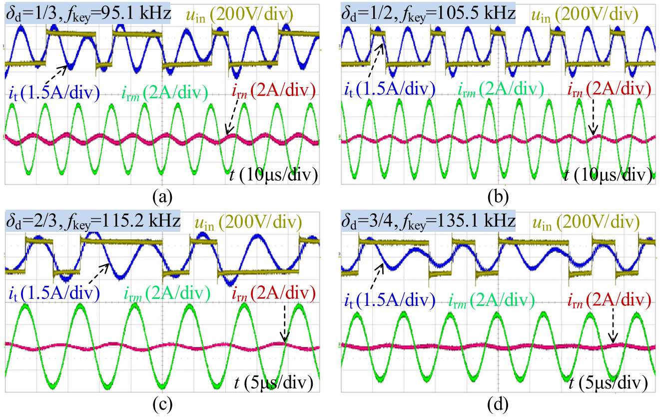

Fig. 16. Measured waveforms of the multi-objective WPT system using proposed soft-switching PFM. (a) $\delta_d = 1/3, f_{\rm key} = 95.1$ kHz. (b) $\delta_d = 1/2, f_{\rm key} = 105.5$ kHz. (c) $\delta_d = 2/3, f_{\rm key} = 115.2$ kHz. (d) $\delta_d = 3/4, f_{\rm key} = 135.1$ kHz.

Fig. 14(a) shows the THDs of the authorized receiver current under the PSC and the PFM. Although the use of PFM slightly increases the THD as compared with the use of PSC, the corresponding THD can be always suppressed below 2.29% for full-range low-frequency soft switching, thus causing insignificant output fluctuations. Fig. 14(b) shows the comparison of various power losses with the same proportion factor in both the PFM and the PSC. Due to the harmonic losses, using the PFM causes slightly higher losses on the inductors, capacitors, and diode rectifier than using the PSC. Nevertheless, the reduction of switching loss of the PFM will outweigh the harmonic losses so that the overall power loss can be reduced while achieving the full-range soft switching.

B. *Experimental Results*

To verify its feasibility of the proposed full-range soft-switching PFM-WPT scheme, a prototype is built for experimental demonstration, as shown in Fig. 15. By using the soft-switching PFM incorporating with different operating frequencies $f_{\rm key}$ and duty ratios δ_d, Fig. 16 shows the measured waveforms of the input voltage $u_{\rm in}$, transmitter current i_t, authorized receiver current i_{rm} and unauthorized one i_{r1}. Since the modulated input voltage can energize the transmitter current slightly before the zero-crossing points with ZVS, the proposed PFM technology can competently implement the high-efficiency WPT while maintaining full-range soft-switching operation during wireless power control. Also, the authorized receiver current with an approximately constant magnitude is much larger than the unauthorized ones. These measured results well confirm the oscillation frequency invariance, the insignificant output fluctuations and the switching frequency suppression, and well agree with their theoretical analyses.

Furthermore, the proposed full-range soft-switching PFM is applied to implement wireless energy selectivity. When the left lateral receiver is selected to harvest wireless power, Fig. 17(a) shows the measured waveforms of the modulated input voltage u_{in}, transmitter current i_t, receiver currents i_{rk}, and output voltages u_{ok}. The unselected receivers can harvest insignificant levels of wireless power, and generate extremely low resonant currents (0.248 A, 0.121 A) and output voltages (2.23 V, 0.928 V), which are far less than the 2.442-A resonant current and 20.80-V output voltage of the left lateral selected receiver. Fig. 17(b) shows the measured waveforms of the PFM-WPT system when the middle receiver is selected. The selected receiver can pick up the vast majority of total transmitted wireless power, and generate the resonant current of 1.989 A and output voltage of 16.83 V, much larger than the resonant currents (0.180 A, 0.147 A) and output voltages (1.62 V, 1.41 V) in the unselected ones. For wireless energy security by using the chaotic PFM, the measured waveforms of the output voltages and authorized receiver current are shown in Fig. 17(c). The security keys, f_{key} and t_{key}, both are chaotically encrypted. With knowledge of the 2-D chaotic security keys, only the authorized receiver can decrypt and pick up nearly all the encoded wireless energy packages and generate the output voltage of 19.89 V, while the unauthorized ones fail to decrypt and generate insignificant output voltages of 1.39 and 0.834 V. Only 0.66% of the total transmitted wireless power is decrypted and stolen. The varying widths of output voltage u_{om} indicate that the duration (t_{key}) of each f_{key} chaotically varies, as shown Fig. 17(c). When the security keys change, Fig. 17(d) shows the transient energy transfer process. The varying pulsewidths of input voltage u_{in} indicate that the security keys and thus the modulated frequency dynamically varies. It confirms that the use of proposed PFM technology can competently realize wireless energy selectivity and security with a full-range soft-switching state.

For simultaneously powering multiple receivers with good alignment, Fig. 18(a) shows the measured waveforms of the proposed multiobjective PFM-WPT system. The PFM technique can enable effective power transmission to the selected receivers *1* and *m*. The selected receivers can harvest almost all the wireless energy, and generate much larger resonant currents (1.339 A, 1.642 A) and output voltages (11.98 V, 14.63 V), while the unselected one can only generate insignificant values of 0.112 A and 0.956 V. As shown in Fig. 18(b), when the receivers suffer from 50% misalignment, the proposed PFM-based technique can simultaneously enable effective power transmission to multiple receivers while withstanding such serious misalignment. The unselected receiver can only pick up insignificant wireless

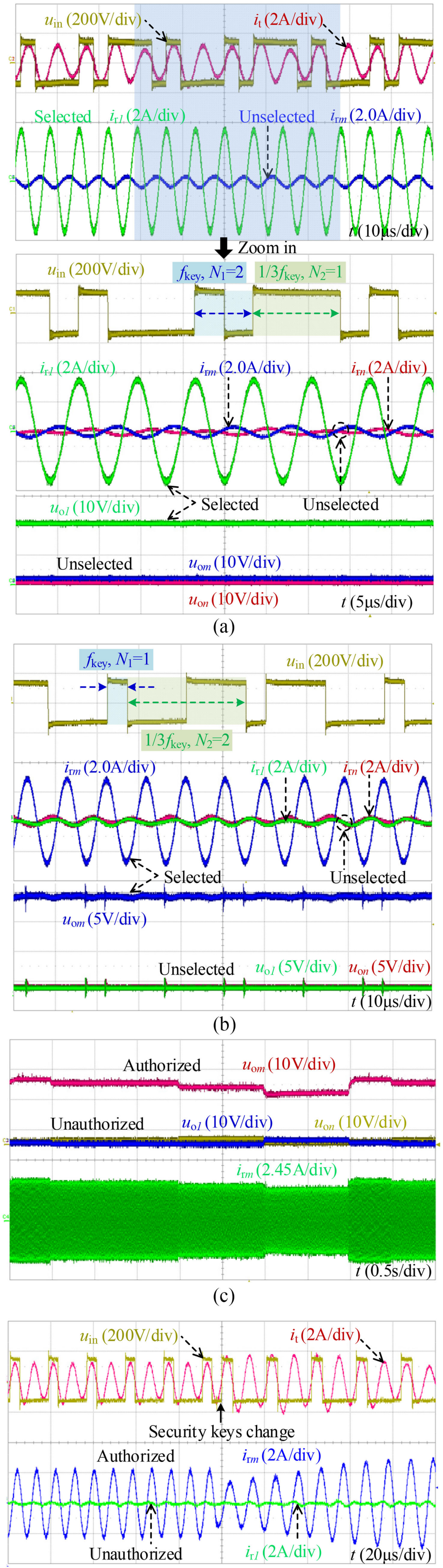

(a)

(b)

(c)

(d)

Fig. 17. Measured waveforms of proposed soft-switching PFM-WPT system. (a) Wireless energy selectivity when left lateral receiver selected. (b) Wireless energy selectivity when middle receiver selected. (c) Wireless energy security. (d) Transient energy transfer process when the security keys change.

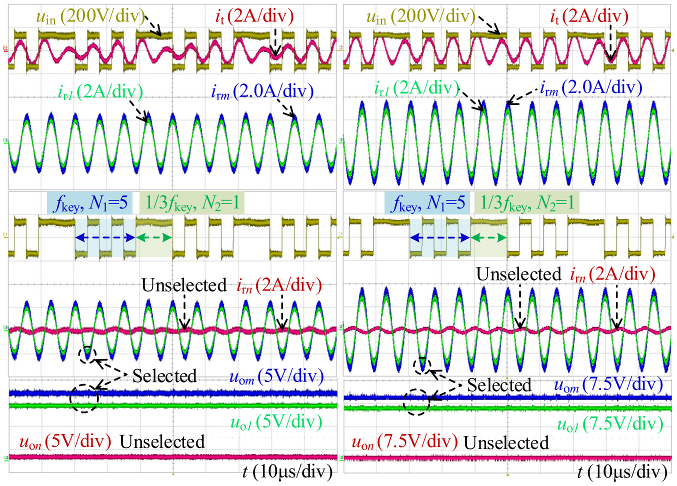

(a) (b)

Fig. 18. Measured waveforms of proposed simultaneously multiobjective PFM-WPT. (a) No misalignment. (b) 50% misalignment.

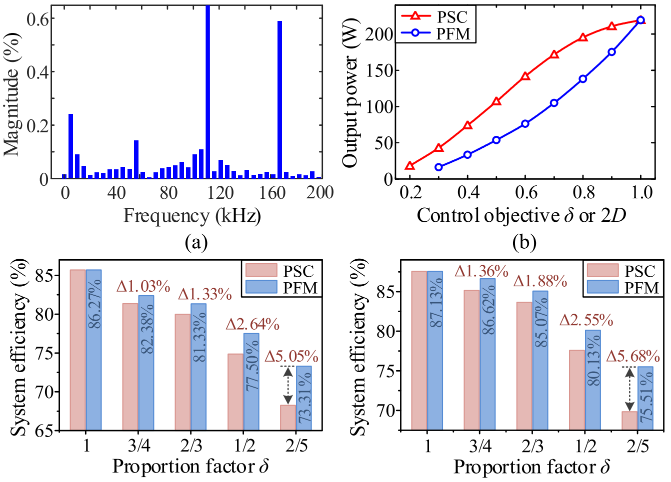

(a) (b) (c) (d)

Fig. 19. Measured characteristics of proposed full-range soft-switching PFM-WPT system. (a) FFT result of receiver current. (b) Wireless energy controllability. (c) Overall system efficiencies when middle receiver selected. (d) Overall system efficiencies when lateral receiver selected.

power, and generate the 0.112-A resonant current and 0.956-V output voltage, which are far less than the currents (1.339 A, 1.642 A) and voltages (11.98 V, 14.63 V) in the selected receivers.

Finally, Fig. 19(a) shows the analysis result of the authorized receiver current by using the fast Fourier transform. Its THD is only 2.74%, which further quantitatively confirms the insignificant output fluctuations in the proposed PFM-WPT system. By applying the PSC and the proposed soft-switching PFM, Fig. 19(b)–(d) shows the measured output powers and overall system efficiencies with respect to their respective control objectives of D and δ. In Fig. 19(b), two output powers monotonically decrease with the decreasing values of control objectives, which well agrees with the wireless energy controllability, as shown in Fig. 8. In Fig. 19(c), the multiobjective WPT system using two control methods have the same system efficiency of 86.27% before activating wireless power adjustment. Once activating equal power adjustment with $\delta = \sin(D\pi)$, however, the multiobjective WPT system using the proposed full-range soft-switching PFM can achieve a higher overall system efficiency, improved by up to 5.05% as compared with that using the PSC. Essentially, the main difference between the lateral and middle coils is reflected in the slightly different mutual inductances. When the lateral receiver is selected to pick up wireless power with a higher frequency f_{key}, the PFM can still improve the system efficiency by up to 5.68% as compared with the PSC in Fig. 19(d). Hence, the proposed full-range soft-switching PFM technology can effectively suppress the power losses and thus improve the system efficiency.

VI. CONCLUSION

In this article, a soft-switching PFM-WPT technology has been proposed and then implemented for high-efficiency wireless energy controllability, selectivity, and security. In contrast to the conventional PSC, the proposed soft-switching PFM technology can guarantee full-range soft-switching operation and reduce the switching frequency during wireless power regulation, thus effectively mitigating the power and efficiency losses. It can be readily implemented in various applications using the conventional constant-frequency WPT, selective WPT, and emerging energy-encrypted WPT with superior controllability, selectivity, and security. The system efficiency of a multiobjective WPT prototype using the proposed soft-switching PFM can reach 86.27% at 220-W output power and 135-mm transfer distance. The proposed soft-switching PFM can effectively improve the system efficiency by up to 5.68% than the PSC once activating power regulation. Theoretical analysis, computer simulation, and hardware experimentation are given to verify the feasibility of proposed full-range soft-switching PFM-WPT system.

APPENDIX A

A. *Proof of Optimal Frequency Modulation*

The PFM inverter output is essentially a piecewise function, which can be written in the form of Fourier series

$$u_{\text{in}}(t) = \begin{cases} \frac{4E}{\pi}\sum_{n_F=1}^{\infty}\frac{\sin[(2n_F-1)\omega_{2n-1}t]}{2n_F-1}, & \omega_{2n-1}=\frac{\omega_{\text{key}}}{2n-1} \\ \frac{4E}{\pi}\sum_{n_F=1}^{\infty}\frac{\sin[(2n_F-1)\omega_{2n+1}t]}{2n_F-1}, & \omega_{2n+1}=\frac{\omega_{\text{key}}}{2n+1} \end{cases} \tag{A1}$$

where ω_{2n-1} and ω_{2n+1} are the modulated switching angular frequencies and also the fundamental angular frequencies of two piecewise outputs $u_{\text{in\_PFM}}$. It contains no $2n_F$th harmonics and subharmonics. Assuming modulated at the even-number frequency dividers of $f_{\text{key}}/(2n)$, $u_{\text{in\_PFM}}$ will contain only $(2n_F-1)$th harmonics, namely the $[(2n_F-1)/2n]$th components. Due to $(2n_F-1)/2n \neq 1$ $(n_F,\, n \in \mathbb{Z}^+)$, their angular frequencies can never equal ω_{key}. The PFM will always fail to achieve effective WPT because of the mismatched frequencies. However, modulated at odd-number frequency dividers of $f_{\text{key}}/(2n \pm 1)$, $u_{\text{in\_PFM}}$ contains the $(2n_F - 1)$th harmonics whose angular frequencies equal ω_{key} when $(2n_F - 1)/(2n \pm 1) = 1$. Hence, two modulated piecewise outputs can both effectively energize the WPT. In the PFM-WPT, we actually utilize the fundamental and the odd-order harmonics of $u_{\text{in\_PFM}}$ rather than the even-order ones. Consequently, turning ON or OFF occurs at every odd-number half-cycle for effective WPT with soft switching.

For verifying the optimality of $f_{\text{key}}/(2n \pm 1)$, modulating at different switching frequencies will generate different output vectors of wireless power. If the targeted vector equals a specific output vector modulated at one fixed frequency, the PFM involves only one modulated frequency. Otherwise, two adjacent odd-number frequency dividers of $f_{\text{key}}/(2n \pm 1)$, such as f_{key} and $f_{\text{key}}/3$, should be chosen, and the system generates two most even output vectors to composite the targeted one. It can contribute to the lowest output fluctuations. If two nonadjacent frequencies are chosen, such as f_{key} and $f_{\text{key}}/5$, the system will produce two less even output vectors for composition, thus causing larger output fluctuations. Hence, the proposed PFM involves two optimal modulated frequencies of $f_{\text{key}}/(2n \pm 1)$.

B. Proof of Oscillation Frequency Invariance

Since the $(2n \pm 1)$th harmonic frequencies of two piecewise PFM outputs in (A1) equal the system innate frequency of f_{key}, the WPT system is piecewisely powered by these $(2n \pm 1)$th harmonics. For example, when the modulated frequency is $f_{\text{key}}/3$, the 3rd harmonic of the piecewise PFM output will effectively energize the WPT system. Thus, the current frequency remains as f_{key}. The bidirectional conduction of the GaN switches will facilitate the resonant current to freewheel for maintaining such frequency invariance.

With a variable duty ratio δ_d, (A1) can be equivalently expressed in an average Fourier series

$$\begin{aligned} u_{\text{in\_PFM}}(t) &= \frac{\delta_d n_1}{\delta_d n_1 + (1-\delta_d)\, n_2} \frac{4E}{\pi} \sum_{n_F=1}^{\infty} \frac{\sin\left[(2n_F - 1)\omega_{2n-1} t\right]}{2n_F - 1} \\ &\quad + \frac{(1-\delta_d)\, n_2}{\delta_d n_1 + (1-\delta_d)\, n_2} \frac{4E}{\pi} \sum_{n_F=1}^{\infty} \frac{\sin\left[(2n_F - 1)\omega_{2n+1} t\right]}{2n_F - 1} \end{aligned} \tag{A2}$$

where $n_1 = 2n - 1$ and $n_2 = 2n + 1$. The n_1th and n_2th harmonics of trigonometric function terms can both construct the fundamental (f_{key}) component for equivalently powering the WPT system as given by

$$\begin{aligned} u_{\text{in\_PFM},1}(t) &= \frac{\delta_d n_1}{\delta_d n_1 + (1-\delta_d)\, n_2} \frac{4E}{n_1 \pi} \sin\left(n_1 \omega_{2n-1} t\right) \\ &\quad + \frac{(1-\delta_d)\, n_2}{\delta_d n_1 + (1-\delta_d)\, n_2} \frac{4E}{n_2 \pi} \sin\left(n_2 \omega_{2n+1} t\right) \\ &= \frac{1}{\delta_d n_1 + (1-\delta_d)\, n_2} \frac{4E}{\pi} \sin\left(\omega_{\text{key}} t\right). \end{aligned} \tag{A3}$$

More generally, the rms value and the proportion factor of the n_Fth harmonic can be written as

$$\begin{aligned} U_{\text{in\_PFM},n_F} &= \frac{2\sqrt{2}E/\left(n_F \pi\right)}{\delta n_1 + (1-\delta)\, n_2} \\ \delta_{\text{PFM},n_F} &= \frac{1/n_F}{\delta_d n_1 + (1-\delta_d)\, n_2}. \end{aligned} \tag{A4}$$

The system characteristics are dominantly determined by the fundamental (f_{key}) component. Actually, $U_{\text{in\_PFM}} = U_{\text{in\_PFM},1}$ and $\delta = \delta_{\text{PFM},1}$. Thus, the transmitter current can be expressed as

$$i_t(t) = \frac{u_{\text{in\_PFM},1}(t)}{Z_{\text{in}}} = \frac{1}{\delta_d n_1 + (1-\delta_d)\, n_2} \frac{4E}{\pi Z_{\text{in}}} \sin\left(\omega_{\text{key}} t\right). \tag{A5}$$

The fundamental PFM output $U_{\text{in\_PFM}}$ will energize the WPT system to resonate at the innate frequency of f_{key}, thus the system oscillation frequency can remain the same regardless of the modulated voltage changes. With a specific load, there are $I_{\text{target}} = \delta I_{\text{rated}}$ and $P_{\text{target}} = \delta^2 P_{\text{rated}}$ as listed in Table II.

With the variable of D, the switching phase angles of the PFM can be accordingly derived as

$$\begin{cases} \alpha_{\omega_{2n-1},n_F} = n_F \left(\frac{\pi}{2} - D\pi\right) |_{D=0.5}\ , \\ \alpha_{\omega_{2n-1},n_1} = n_1 \left(\frac{\pi}{2} - D\pi\right) |_{D=0.5} = 0^\circ \\ \alpha_{\omega_{2n+1},n_F} = n_F \left(\frac{\pi}{2} - D\pi\right) |_{D=0.5}\ , \\ \alpha_{\omega_{2n+1},n_2} = n_2 \left(\frac{\pi}{2} - D\pi\right) |_{D=0.5} = 0^\circ. \end{cases} \tag{A6}$$

It indicates that the phase difference can keep zero between the PFM switching and the transmitter current. Although the frequencies are modulated between $f_{\text{key}}/(2n \pm 1)$, the switches can be turned ON/OFF exactly at or slightly before the zero-crossing point of the transmitter current for soft switching. It further verifies that the transmitter frequency can keep constant, and essentially reveals the system oscillation frequency invariance.

APPENDIX B

The PFM function generator aims to generate a variable-frequency piecewise sine wave. Defining the prior one as γ_{f2n-1} and the latter one as γ_{f2n+1}, the two sinusoidal signals are expressed as

$$\begin{cases} \gamma_{f2n-1} = \sin\left\{(-1)^{\text{mod}(k_1,\,2)} 2\pi f_{2n-1}\left[t - k_1/\left(2f_{\text{key}}\right)\right]\right\} \\ \gamma_{f2n+1} = \sin\left\{(-1)^{\text{mod}(k_2,\,2)} 2\pi f_{2n+1}\left[t - k_2/\left(2f_{\text{key}}\right)\right]\right\} \end{cases} \tag{B1}$$

where

$$\begin{cases} k_1 = (k-1)\left[(2n-1)\, N_1 + (2n+1)\, N_2\right] \\ k_2 = k\,(2n-1)\, N_1 + (k-1)\,(2n+1)\, N_2. \end{cases} \tag{B2}$$

The algorithm of the PFM function generator is depicted in Fig. 20, where t is the discrete time of system clock, and the frequency f_{key} can be updated in real time. It can readily be programmed to realize in both the computer simulation and digital signal processor (DSP) controller. In particular, for the DSP, the interrupt of the PWM module is used to produce the

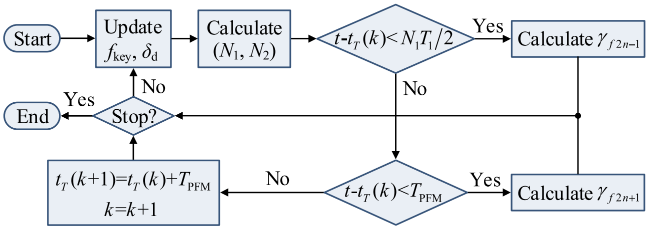

Fig. 20. Algorithm of proposed PFM function generator.

desired PFM gate signals. The interrupt frequency is set as $2f_{\mathrm{key}}$ updated in real time. When the interrupt count equals N_1 or (N_1+N_2), alternately configuring the interrupt triggered at the ($2n \pm 1$)th event is to generate the prior and latter PFM gate signals, respectively. In the processing program of PWM interrupt, all the gate signals will be toggled.

REFERENCES

[1] G. A. Covic and J. T. Boys, "Inductive power transfer," *Proc. IEEE*, vol. 101, no. 6, pp. 1276–1289, Jun. 2013.

[2] C. C. Mi, G. Buja, S. Y. Choi, and C. T. Rim, "Modern advances in wireless power transfer systems for roadway powered electric vehicles," *IEEE Trans. Ind. Electron.*, vol. 63, no. 10, pp. 6533–6545, Oct. 2016.

[3] S. Y. Jeong, H. G. Kwak, G. C. Jang, S. Y. Choi, and C. T. Rim, "Dual-purpose nonoverlapping coil sets as metal object and vehicle position detections for wireless stationary EV chargers," *IEEE Trans. Power Electron.*, vol. 33, no. 9, pp. 7387–7397, Sep. 2018.

[4] X. Dai, J. Jiang, and J. Wu, "Charging area determining and power enhancement method for multiexcitation unit configuration of wirelessly dynamic charging EV system," *IEEE Trans. Ind. Electron.*, vol. 66, no. 5, pp. 4086–4096, May 2019.

[5] Y. Zhang, T. Lu, Z. Zhao, F. He, K. Chen, and L. Yuan, "Selective wireless power transfer to multiple loads using receivers of different resonant frequencies," *IEEE Trans. Power Electron.*, vol. 30, no. 11, pp. 6001–6005, Nov. 2015.

[6] Y. J. Kim, D. Ha, W. J. Chappell, and P. P. Irazoqui, "Selective wireless power transfer for smart power distribution in a miniature-sized multiple-receiver system," *IEEE Trans. Ind. Electron.*, vol. 63, no. 3, pp. 1853–1862, Mar. 2016.

[7] Z. Zhang, K. T. Chau, C. Qiu, and C. Liu, "Energy encryption for wireless power transfer," *IEEE Trans. Power Electron.*, vol. 30, no. 9, pp. 5237–5246, Sep. 2015.

[8] W. Liu, K. T. Chau, C. H. T. Lee, C. Jiang, and W. Han, "A switched-capacitorless energy-encrypted transmitter for roadway-charging electric vehicles," *IEEE Trans. Magn.*, vol. 54, no. 11, pp. 1–6, Nov. 2018.

[9] Y. Jiang, L. Wang, Y. Wang, J. Liu, X. Li, and G. Ning, "Analysis, design, and implementation of accurate ZVS angle control for EV battery charging in wireless high-power transfer," *IEEE Trans. Ind. Electron.*, vol. 66, no. 5, pp. 4075–4085, May 2019.

[10] C. Jiang, K. T. Chau, C. H. T. Lee, W. Han, W. Liu, and W. H. Lam, "A wireless servo motor drive with bidirectional motion capability," *IEEE Trans. Power Electron.*, vol. 34, no. 12, pp. 12001–12010, Dec. 2019.

[11] A. Berger, M. Agostinelli, S. Vesti, J. A. Oliver, J. A. Cobos, and M. Huemer, "A wireless charging system applying phase-shift and amplitude control to maximize efficiency and extractable power," *IEEE Trans. Power Electron.*, vol. 30, no. 11, pp. 6338–6348, Nov. 2015.

[12] C. Jiang, K. T. Chau, W. Liu, C. Liu, W. Han, and W. H. Lam, "An LCC compensated multiple-frequency wireless motor system," *IEEE Trans. Ind. Inform.*, vol. 15, no. 11, pp. 6023–6034, Nov. 2019.

[13] W. Zhong and S. Y. R. Hui, "Maximum energy efficiency operation of series-series resonant wireless power transfer systems using on-off keying modulation," *IEEE Trans. Power Electron.*, vol. 33, no. 4, pp. 3595–3603, Apr. 2018.

[14] W. Liu, J. Zhang, and R. Chen, "Modelling and control of a novel zero-current-switching inverter with sinusoidal current output," *IET Power Electron.*, vol. 9, no. 11, pp. 2205–2215, Sep. 2016.

[15] H. Li, S. Chen, J. Fang, Y. Tang, and M. de Rooij, "A low-subharmonic, full-range, and rapid pulse density modulation strategy for ZVS full-bridge converters," *IEEE Trans. Power Electron.*, vol. 34, no. 9, pp. 8871–8881, Sep. 2019.

[16] X. Ju, L. Dong, X. Huang, and X. Liao, "Switching technique for inductive power transfer at high-*Q* regimes," *IEEE Trans. Ind. Electron.*, vol. 62, no. 4, pp. 2164–2173, Apr. 2015.

[17] H. Zeng, S. Yang, and F. Z. Peng, "Design consideration and comparison of wireless power transfer via harmonic current for PHEV and EV wireless charging," *IEEE Trans. Power Electron.*, vol. 32, no. 8, pp. 5943–5952, Aug. 2017.

[18] W. Liu, K. T. Chau, C. H. T. Lee, C. Jiang, W. Han, and W. H. Lam, "Multi-frequency multi-power one-to-many wireless power transfer system," *IEEE Trans. Magn.*, vol. 55, no. 7, pp. 1–9, Jul. 2019.

[19] C. T. Rim and G. H. Cho, "Quantum transformation: The analysis of quantum rectifier-inverters," in *Proc. Conf. Rec. IEEE Ind. Appl. Soc. Annu. Meeting*, 1989, pp. 1081–1085.

[20] G. B. Joung, J. G. Cho, and G. H. Cho, "A generalized quantum resonant converter using a new quantum resonant module," *IEEE Trans. Power Electron.*, vol. 7, no. 4, pp. 666–672, Oct. 1992.

[21] Y. Lim and J. Park, "A novel phase-control-based energy beamforming techniques in nonradiative wireless power transfer," *IEEE Trans. Power Electron.*, vol. 30, no. 11, pp. 6274–6287, Nov. 2015.

[22] W. Meng, F. Zhang, Z. Fu, and G. Dong, "High dv/dt noise modeling and reduction on control circuits of GaN-based full bridge inverters," *IEEE Trans. Power Electron.*, vol. 34, no. 12, pp. 12246–12261, Dec. 2019.

[23] J. Choi, D. Tsukiyama, Y. Tsuruda, and J. M. R. Davila, "High-frequency, high-power resonant inverter with eGaN FET for wireless power transfer," *IEEE Trans. Power Electron.*, vol. 34, no. 12, pp. 12246–12261, Dec. 2019.

[24] Sun, H. Zhang, A. P. Hu, C. Tang, and L. Xiang, "The recognition and control of nonideal soft-switching frequency for wireless power transfer system based on waveform identification," *IEEE Trans. Power Electron.*, vol. 32, no. 8, pp. 6617–6627, Aug. 2017.

[25] M. Hénon, "A two-dimensional mapping with a strange attractor," *Comm. Math. Phys.*, vol. 50, no. 1, pp. 69–77, Feb. 1976.

Wei Liu (S'17) received the B.Eng. degree in electrical engineering and automation and the M.Eng. degree in electrical engineering from the China University of Petroleum (East China), Qingdao, China, in 2014 and 2017, respectively. He is currently working toward the Ph.D. degree in electrical and electronic engineering at the Department of Electrical and Electronic Engineering, The University of Hong Kong, Hong Kong.

He was a Visiting Researcher with the Nanyang Technological University, Singapore, in 2019. His research interests include power electronics, wireless power transfer techniques, and electric vehicle technologies.

K. T. Chau (M'89–SM'04–F'13) received the B.Sc. (Eng.), M.Phil., and Ph.D. degrees in electrical and electronic engineering from The University of Hong Kong, Hong Kong, in 1988, 1991, and 1993, respectively.

Since 1995, he has been with The University of Hong Kong, where he is currently a Professor with the Department of Electrical and Electronic Engineering. He is the author of nine books and more than 300 journal papers. His research interests include electric and hybrid vehicles, power electronics and drives, and renewable energies.

Dr. Chau is a Fellow of the Institution of Engineering and Technology (IET), U.K., and of the Hong Kong Institution of Engineers. He is currently also a Co-Editor for the *Journal of Asian Electric Vehicles*. He is a Chartered Engineer in Hong Kong. He was the recipient of the Changjiang Chair Professorship from the Ministry of Education, China, and the Environmental Excellence in Transportation Award for Education, Training, and Public Awareness from the Society of Automotive Engineers International.

Christopher H. T. Lee (M'12–SM'18) received the B.Eng. (First Class Hons.) and Ph.D. degrees in electrical engineering from The University of Hong Kong, Hong Kong, in 2009 and 2016, respectively.

He is currently an Assistant Professor in power engineering with the Nanyang Technological University, Singapore, a Visiting Assistant Professor with the Massachusetts Institute of Technology, Cambridge, MA, USA, and an Honorary Assistant Professor in the *alma mater*. His research interests include electric machines and drives, renewable energies, and electric vehicle technologies. In these areas, he has published one book, three book chapters, and about 70 referred papers.

Wei Han (S'16) received the B.Eng. degree in electrical engineering and automation from Northeastern University, Shenyang, China, in 2014, and the M.Eng. degree in electrical and electronic engineering in 2015, from The University of Hong Kong, Hong Kong, where he is currently working toward the Ph.D. degree in electrical and electronic engineering at the Department of Electric and Electronic Engineering.

His research interests include wireless power transfer techniques, power electronics, and renewable energies.

Xiaoyang Tian (S'18) received the B.Eng. degree in electrical engineering and automation from Hangzhou Dianzi University, Hangzhou, China, in 2015, and the M.Eng. degree in electrical engineering from North China Electric Power University, Baoding, China, in 2018. He is currently working toward the Ph.D. degree in electrical and electronic engineering at the Department of Electrical and Electronic Engineering, The University of Hong Kong, Hong Kong.

His research interests include wireless power transfer techniques, power electronics, and electric vehicle technologies.

W. H. Lam (SM'09) was born in Hong Kong. He received the B.Sc. degree in computer and communication engineering from the University of Essex, Colchester, U.K., in 1983, the M.Sc. degree in telecommunication engineering from the Imperial College, University of London, London, U.K., in 1984, and the Ph.D. degree in digital mobile radio communications from the University of Southampton, Southampton, U.K., in 1988.

In 1991, he joined the Department of Electrical and Electronic Engineering, University of Hong Kong. He has authored or coauthored more than 70 technical publications in the field of digital cellular mobile radio communications and the intelligent transport systems (ITS). He was the Chairman and Organizer of a series of regional conferences on mobile radio communications and a Distinguished Speaker and Chairperson at several international conferences and meetings. His current research interests include the next generation digital mobile radio and spread spectrum communications systems, ITS, power electronics, and drives.

Dr. Lam was the recipient of the SERC CASE Award from the University of Southampton.